J Geod
DOI 10.1007/s00190-016-0968-8

ORIGINAL ARTICLE

CODE's five-system orbit and clock solution—the challenges of multi-GNSS data analysis

Lars Prange[1] · **Etienne Orliac**[1] · **Rolf Dach**[1] · **Daniel Arnold**[1] · **Gerhard Beutler**[1] · **Stefan Schaer**[2] · **Adrian Jäggi**[1]

Received: 9 December 2015 / Accepted: 19 October 2016

Abstract This article describes the processing strategy and the validation results of CODE's MGEX (COM) orbit and satellite clock solution, including the satellite systems GPS, GLONASS, Galileo, BeiDou, and QZSS. The validation with orbit misclosures and SLR residuals shows that the orbits of the new systems Galileo, BeiDou, and QZSS are affected by modelling deficiencies with impact on the orbit scale (e.g., antenna calibration, Earth albedo, and transmitter antenna thrust). Another weakness is the attitude and solar radiation pressure (SRP) modelling of satellites moving in the orbit normal mode—which is not yet correctly considered in the COM solution. Due to these issues, we consider the current state COM solution as preliminary. We, however, use the long-time series of COM products for identifying the challenges and for the assessment of model-improvements. The latter is demonstrated on the example of the solar radiation pressure (SRP) model, which has been replaced by a more generalized model. The SLR validation shows that the new SRP model significantly improves the orbit determination of Galileo and QZSS satellites at times when the satellite's attitude is maintained by yaw-steering. The impact of this orbit improvement is also visible in the estimated satellite clocks—demonstrating the potential use of the new generation satellite clocks for orbit validation. Finally, we point out further challenges and open issues affecting multi-GNSS data processing that deserves dedicated studies.

✉ Lars Prange
lars.prange@aiub.unibe.ch

[1] Astronomical Institute of the University of Bern, Sidlerstrasse 5, 3012 Bern, Switzerland

[2] Bundesamt für Landestopografie swisstopo, Seftigenstrasse 264, 3084 Wabern, Switzerland

Keywords IGS · CODE · Multi-GNSS · ECOM · Solar radiation pressure model · Orbit determination · Satellite clock

1 Introduction

The International GNSS Service (IGS, Dow et al. 2009) has been providing products based on the measurements of Global Navigation Satellite Systems (GNSS) collected by a global permanent station network on an operational basis for more than 20 years. The Center for Orbit Determination in Europe (CODE, Dach et al. 2015) contributes to the IGS as a global analysis center (AC). In 2012, the IGS initiated the Multi-GNSS EXperiment (MGEX, Montenbruck et al. 2013) to prepare the service for new GNSS, such as Galileo and BeiDou, and for Regional Navigation Satellite Systems (RNSS), such as the Quasi-Zenith Satellite System (QZSS) and the Indian Regional Navigation Satellite System (IRNSS). The new systems, but also the established GNSS GPS and GLONASS, offer new signals, observation types, and types of spacecrafts (some equipped with new types of satellite clocks). An increasing user request motivates CODE and other IGS ACs to participate in the MGEX.

Initially, the focus of CODE's MGEX-related activity was on the step-wise extension of software and processing chains to enable the inclusion of new satellite systems and of GNSS measurements stored in version 3 of the Receiver INdependent EXchange data format (RINEX3, see MacLeod and Agrotis 2013, for the format description). 2014 was the first year when five satellite systems, namely GPS, GLONASS, Galileo, BeiDou, and QZSS, were included in CODE's MGEX (COM) solution during the whole year. The background models and processing stan-

Published online: 24 November 2016

dards are adopted from CODE's RAPID scheme for the IGS (Dach et al. 2015). This includes the Empirical CODE Orbit Model, a solar radiation pressure (SRP) model, which was originally introduced by Beutler et al. (1994) for GPS satellites with yaw-steering attitude. A reduced version of this model was proposed by Springer et al. (1999) (called ECOM1 in this work). We consider the current development state as preliminary and see it as a starting point for the next phase of our MGEX effort: the analysis of the extended time series of COM products allows us to identify weaknesses that our established IGS processing strategy has w.r.t. the new systems and data and to study the impact of model changes. The identification of possible challenges for a multi-GNSS processing is one of the goals of this work.

Validation results shown by Steigenberger et al. (2015), but also analyses performed by, e.g., Prange et al. (2016) and Uhlemann et al. (2016), on their own MGEX products revealed that one of the most noticeable issues of the orbits of current Galileo IOV (In Orbit Validation) products are periodic orbit errors, whose amplitudes vary as a function of the elevation angle β of the Sun above the satellite orbital planes and that these orbit errors are mapped into the satellite clock corrections. Montenbruck et al. (2015) demonstrated that the orbit errors with a once-per-orbit-revolution (1/rev) signature can be significantly reduced, if the ECOM1 is used together with an a priori box model. The correlation between the radial orbit errors and the β-angle was also reported for QZSS (Steigenberger and Kogure 2014). At the same time, new SRP models were developed with the goal to reduce draconitic errors in the time series of IGS products which are based on GPS and GLONASS data. Among them is a revised version of CODE's empirical orbit model (called ECOM2 in this work, Arnold et al. 2015). Like ECOM1, ECOM2 is designed for satellites whose attitude is maintained by yaw-steering. The main improvement of ECOM2 over ECOM1 is the introduction of even (2/rev) and (4/rev) periodic terms in the direction of direct solar radiation (Sun–Earth direction or D-axis of the ECOM decomposition). Like other modern SRP models, such as the ones introduced by Ziebart (2004), Ikari et al. (2013), Rodriguez-Solano et al. (2014), Springer et al. (2014), Montenbruck et al. (2015), or Steigenberger et al. (2015), ECOM2 is able to consider the variation of the direct solar radiation pressure within an orbit revolution caused by the variation of the illuminated cross-section of a rotating, elongated satellite body. The ECOM1, in contrast, assumes that the force in the direction of direct solar radiation (D axis of the ECOM decomposition) is constant within an orbit arc, which would be true for spherical satellite bodies and is a good approximation for cubic satellite bodies. Compared with the (semi-)analytical models, empirical orbit models, such as the ECOM2, have the advantage of being independent from knowing the satellite shape, mass, and surface properties (Arnold et al. 2015). As the properties of new satellite systems are not always known sufficiently well and different satellite types with elongated bodies (at least GLONASS, Galileo, and QZSS) are involved in the MGEX, the ECOM2 SRP model is a promising alternative to the ECOM1 and to type-specific analytical SRP models in a multi-GNSS environment. Therefore, the ECOM1 was replaced by the ECOM2 in our COM solution in early 2015 and the data of 2014 have been reprocessed. The evaluation of the impact of this model change is another major goal of this work.

We start with the description of the data basis and station network used for our MGEX analysis in Sect. 2. Section 3.1 describes the processing strategy for the precise orbit determination (POD), which is used to generate the operational COM orbit solution but also the reprocessed sets of orbits from 2014 based on the ECOM1 and ECOM2 SRP models, respectively. Introducing the POD results, consistent sets of satellite clock corrections are determined as described in Sect. 3.2. The reprocessed COM orbits and clocks are validated in Sect. 4. The results are summarized and discussed in Sect. 5. The work is concluded with Sect. 6.

2 Data basis, network, and satellite constellations

The COM products are based on GNSS measurements stored in RINEX3 data files from the IGS MGEX network and from the EUREF Permanent Network (EPN, Bruyninx et al. 2011) and on data from the IGS network stored in the older format RINEX2 (supporting only GPS and GLONASS). At CODE, the incoming RINEX files are checked for compatibility with the file format. Raw-data statistics are created and made publicly available (Lutz et al. 2013, ftp://ftp.unibe.ch/aiub/mgex/README.TXT).

The observation type summary in Table 1 was extracted from the RINEX3 data monitoring. The table shows the large variety of different observation types available within a time interval of 30 days in 2014. As the COM products are based on a dual-frequency processing, two frequencies are selected per GNSS. The last column in Table 1 tells which observation types are actually used for the COM solution. Signals with a high availability are preferred (except GPS C1C). Apart from the GPS satellite-related bias classically called "P1-C1" differential code bias (DCB, Schaer 2012), the code and phase biases between signals on the same carrier frequency are neglected. For the new GNSS, this limits the resolution rate of integer ambiguity resolution strategies using the Melbourne–Wübbena linear combination. An impact on the estimated satellite clock corrections might be expected as well. The proper handling of all observation biases (including phase biases) is still an open issue and requires further

Table 1 Signals contained in RINEX3 observation files checked at CODE during the time interval DOY (Day Of the Year) 250–280/2014. The system characters in the "Sys" column and the "Signal" designators are in line with the RINEX3 format description. "A": Availability (100% indicates that an observation type was provided by all stations on all days during the time interval). "Use" indicates, which observation types are activated for the COM processing

Sys	Frequency		Signal	A	Use
	Band	MHz	Phase/Code	%	
G	L1	1575.42	L1C/C1C	100	X
			L1W/C1W	17	X
	L2	1227.60	L2W/C2W	95	X
			L2X/C2X	52	X
			L2S/C2S	24	X
			L2L/C2L	11	X
			L2C/C2C	2	X
			L2D/C2D	1	X
	L5	1176.45	L5X/C5X	50	
			L5Q/C5Q	39	
R	G1	1598.0625	L1C/C1C	100	X
		−1608.75	L1P/C1P	54	X
	G2	1242.9375	L2P/C2P	99	X
		−1251.25	L2C/C2C	87	X
E	E1	1575.42	L1X/C1X	55	X
			L1C/C1C	42	X
	E5a	1176.45	L5X/C5X	56	X
			L5Q/C5Q	42	X
	E5b	1207.14	L7Q/C7Q	41	
			L7X/C7X	38	
	E5	1191.795	L8Q/C8Q	44	
	(a+b)		L8X/C8X	35	
C	B1	1561.098	L1I/C1I	54	X
			L2I/C2I	44	X
			L2X/C2X	1	X
	B2	1207.14	L7I/C7I	66	X
			L7X/C7X	2	X
	B3	1268.52	L6I/C6I	61	
			L6X/C6X	1	
J	L1	1575.42	L1C/C1C	100	X
			L1X/C1X	55	X
	L2	1227.60	L2X/C2X	81	X
			L2L/C2L	12	X
			L2S/C2S	2	X
	L5	1176.45	L5X/C5X	79	
			L5Q/C5Q	13	
S	L1	1575.42	L1C/C1C	100	
	L5	1176.45	L5I/C5I	27	

software improvements. The selection of the most suitable signals and linear combinations needs further investigations, as well.

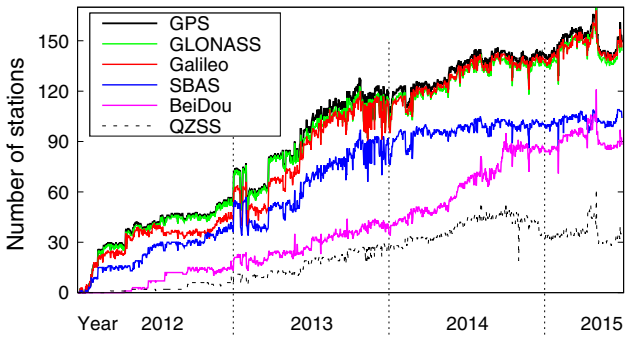

Fig. 1 Number of stations considered in CODE's raw-data monitoring and providing RINEX3 data

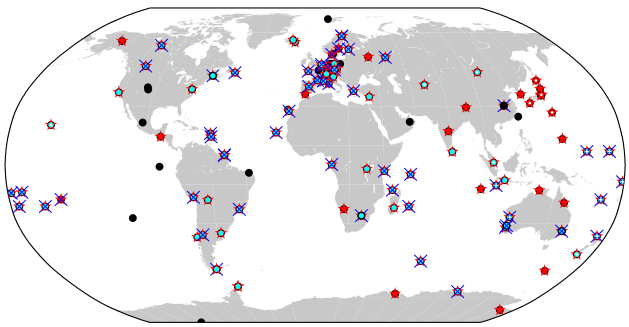

Fig. 2 Distribution of GNSS tracking stations contributing to the CODE MGEX orbit solution on DOY 30/2015. *Black dots* GPS. *Red stars* GLONASS. *Cyan dots* Galileo. *Black X-es* BeiDou. *Small white dots* QZSS

Figure 1 shows that the number of sites providing RINEX3 data increased from about 30 in spring 2012 to about 150 in summer 2015. All stations support GPS, almost all observe GLONASS and Galileo in addition. BeiDou, QZSS, and SBAS are tracked by fewer sites. Although the MGEX network grew worldwide, it is densest in Europe (the EPN sites add to this imbalance). Therefore, we apply a station selection scheme for the COM solution, optimizing the network geometry (i.e., stations close to many others are removed) and the number of observations (i.e., stations providing more observations and supporting several GNSS are preferred). The number of selected stations is limited to 130. Figure 2 shows the station network on DOY 30/2015 after the station selection. Even with the station selection applied, the network density is highest in Europe. GPS, GLONASS, and Galileo are well observed worldwide. QZSS is well supported over East–Asia and the Western Pacific—representing the regions of interest for this RNSS. BeiDou is sufficiently well observed in most parts of the world, except in the Northern Pacific and Northern Asia region. The limited availability of BeiDou tracking data in this part of the world might affect the POD of the regional BeiDou components, namely the IGSO (Inclined Geosyn-

Table 2 Relevant satellite status changes for new GNSS included in the COM solution (late 2013 to mid 2015)

Sat typ	Sat PRNs	Status
Galileo IOV	E11, E12, E19, E20	E20 outage from 27 May to 24 Sept. 2014 and transmitting only on E1 since 25 Sept. 2014
Galileo FOC1	E14, E18	Launch date: 22 Aug. 2014 (wrong orbit);
		Active since: 09 Dec. 2014 (E18) and 17 March 2015 (E14);
		E14 inactive since 12 July 2015
Galileo FOC2	E22, E26	Launch date: 27 March 2015;
		Active since 23 May 2015 (E22), 26 May 2015 (E26);
		E22 inactive since 17 June 2015;
		E26 inactive since 23 July 2015
Galileo FOC3	E24, E30	Launch date: 11 Sept. 2015
BeiDou IGSO	C06, C07, C08, C09, C10	
BeiDou MEO	C11, C12, C13, C14	C13 inactive since 21 Oct. 2014 for unknown reasons
BeiDou3 I1-S	?	Launch date: 30 March 2015
BeiDou3 M1+2	?	Launch date: 25 July 2015
QZSS	J01	Active

chronous Orbit) and the GEO (Geostationary Earth Orbit) satellites.

Table 2 lists satellites included in the COM solution on top of GPS and GLONASS as well as events which have an impact on the COM solution in 2014 and early 2015. For Galileo IOV satellite E20, a power anomaly was reported on 27 May 2014 (Langley 2014), causing a long outage. Since its re-activation E20 is transmitting only on the E1 frequency. It is, therefore, excluded from our dual-frequency processing since then. Already on 23 August 2013, E20's active clock was switched to one of the Rubidium Atomic Frequency Standard (RAFS) clocks (IGS-MGEX 2015). For all other Galileo satellites, a Passive Hydrogen Maser (PHM) was active most of the time in 2014 and 2015. The first two Galileo FOC (Full Operational Capability) satellites were launched into non-nominal orbits (eccentric, low perigee, wrong inclination). After raising the perigee with the thruster engines, the satellites became active in late 2014 and early 2015 (GalileoGNSS 2015), although their orbits are still more eccentric than originally planned. For BeiDou, only the IGSO and MEO (medium Earth orbit) satellites are currently included in the COM products. The MEO satellite C13 became inactive without notification in fall 2014. The new BeiDou3 satellites launched since 2015 are not yet included.

3 CODE MGEX solution strategy

3.1 Orbit product generation

Since 2012, the COM processing scheme has been developed in several steps and is currently able to generate orbits of the five systems GPS, GLONASS, Galileo, BeiDou, and QZSS in a fully integrated way (i.e., data of all satellite systems are processed together and contribute to the common parameters, such as station coordinates, Earth rotation parameters (ERPs), and troposphere parameters). The software package is a development version of the Bernese GNSS Software (Dach et al. 2015). Starting from DOY 145/2012, the estimated orbits and ERPs referring to the middle day of the 3-day-long arc solution are made available at the MGEX product directory of the IGS—since early 2015 on a regular basis with a latency of about two weeks. Details of the COM orbit processing, including the background models, can be found in Table 3.

In the initial phase of MGEX, the COM processing strategy, background models, and processing standards were as far as possible adopted from the existing IGS processing schemes (Dach et al. 2015). In many aspects, however, they suffer from a lack of relevant input information regarding the new systems. This applies, e.g., for the calibrations of the satellite antenna phase center offsets (PCO) and variations (PCV). For Galileo ground-calibrated PCOs and PCVs are used, which are, however, not publicly available. For BeiDou and QZSS PCOs provided by the IGS MGEX (Montenbruck et al. 2015), but no PCV calibrations are used. Meanwhile, estimated PCOs and PCVs are available for BeiDou from Dilssner et al. (2014) and Guo et al. (2016) and estimated PCOs for Galileo are provided by Steigenberger et al. (2016). Note, that also the ground antennas need to be calibrated for the new satellite systems and/or new frequencies.

Models for Earth radiation (albedo) pressure and transmitter antenna thrust are only applied for GPS and GLONASS. Corresponding information for the new systems is not yet published. According to Rodriguez-Solano et al. (2012), the neglect of Earth albedo and antenna thrust causes radial orbit offsets with an approximate size of 1–2 and 0.5 cm, respectively, for GPS satellites. The GPS and GLONASS ambiguity resolution is performed analogue to CODE's IGS solution (see, Dach et al. 2012 for a description). The adaptation of the ambiguity resolution to the new GNSS is still pending. It requires the proper handling of observation biases, which is another open issue. Pseudo-stochastic pulses are only set up for GPS and GLONASS, but not for the new GNSS. The reason is that these parameters might become singular for poorly observed satellites.

Some models are applied to all GNSS, accepting that such simplifications are not always correct. This applies to the satellite attitude, where yaw-steering according to Bar-Sever

Table 3 Specifications of the COM orbit processing

GNSS considered	GPS, GLONASS, Galileo, BeiDou, (MEO and IGSO), QZSS (≈70 SVs in total)
Processing mode	Post-processing, 2 weeks latency
Time span	Since DOY 146/2012 (GPSWEEK 1689)
# of stations	130 (GPS), 110 (GLONASS), 85 (Galileo), 55 (BeiDou), 20 (QZSS)
Processing scheme	Double-difference network processing (observable: phase double differences, ionosphere-free linear combination)
Signals used	See column "Use" in Table 1
Elevation mask	3°; elev.-dependent weighting ($\cos^2(z)$)
Obs. sampling	180 s
Reference frame	IGS08 (until GPSWEEK 1708); IGb08 (since GPSWEEK 1709)
Ionosphere	Model up to 3rd order (Dach et al. 2012)
Sat. antenna model	GPS, GLONASS: PCO and PCV from IGS; Galileo: PCO and PCV from ESA; BeiDou, QZSS: PCO from IGS MGEX
Rec. antenna model	GPS, GLONASS: IGS PCO and PCV; new GNSS: adopted from GPS L1 and L2
Albedo model	GPS, GLONASS: applied; new GNSS: not applied
Transmitter thrust	GPS: applied (Rodriguez-Solano et al. 2012); GLONASS: applied (Dach et al. 2015); new GNSS: not applied
Ambiguity resolution	GPS, GLONASS: active (Dach et al. 2012); new GNSS: enabled, but not tuned
Attitude model	Yaw-steering always assumed for all sat.
Orbit model	Middle day of 3-day-long arc; SRP model: until 2014: ECOM1 (D0,Y0,B0,B1C,B1S)/ since 2015: ECOM2 (D0,Y0,B0,B1C,B1S, D2C,D2S,D4C,D4S), unconstrained; pseudo-stochastic pulses every 12 h in along-track, cross-track, radial for GPS and GLONASS
Product list	Daily orbits (SP3c;15 min) and ERPs
Distribution	ftp://cddis.gsfc.nasa.gov/gnss/products/mgex/

(1996) is always assumed for all satellites. Note that this assumption is not correct during eclipse, which was shown, e.g., by Kouba (2009) for GPS and Dilssner et al. (2011) for GLONASS. Konrad et al. (2007) presented an attitude law for Galileo IOV satellites during their midnight and noon turns. Even larger deviations from the assumed yaw-steering must be expected for the BeiDou and QZSS satellites, switching from yaw-steering to orbit normal attitude mode (i.e., the satellites solar panel axis is aligned normal to the orbital plane; the navigation antenna points to the Earth) at $|\beta|$-angles below 20° in the case of QZS-1 (Ishijima et al. 2009) and about 4° in the case of the BeiDou IGSO and MEO satellites according to Dai et al. (2015). The implementation of the correct attitude laws into our software is a pending issue.

As opposed to a classical GPS and GLONASS solution, including only satellites with more or less circular MEO orbits and an orbit period of about half a day, the five-system COM solution includes satellites with different revolution times, inclinations, and eccentricities. Using the same orbit arc-length and SRP model for all orbit types (as currently done) is another simplification that might possibly not be optimal.

Originally, the ECOM1 SRP model was applied to all satellites. One of the most important model changes in Table 3 was the switch to the more general ECOM2 at the beginning of 2015. In order to study the impact of this model change on the COM orbits, the data of the entire year 2014 have been reprocessed—once using ECOM1 and once using ECOM2. As both SRP models are strictly designed for yaw-steering, it cannot be expected that they work correctly when satellites change to another attitude law (e.g., during eclipse or in orbit normal mode).

The orbit determination of GEO satellites is considered to be especially challenging for different reasons: long revolution time (one day), the static viewing geometry resulting in a poor observability of the orbit parameters, attitude (permanent orbit normal mode), SRP modelling, and frequent satellite maneuvers (see, e.g., Steigenberger et al. 2013). GEO satellites are, therefore, currently excluded from our processing.

3.2 Clock product generation

The COM clock solution is based on a zero-difference processing scheme designed as a back-substitution step. The geometry-related information (orbit parameters, ERPs, station coordinates, and troposphere estimates) is introduced from the COM double-difference solution (see Sect. 3.1) and kept fixed in order to estimate the receiver and satellite clock corrections together with the related biases. The set of biases consists of P1-C1 DCBs (one per GPS satellite and day), intersystem biases (ISB; one per station and day), and of GLONASS interfrequency biases (IFB; one per station, GLONASS satellite, and day). Apart from the GPS P1-C1 DCBs, biases between signals on the same carrier frequency are neglected.

The processing standards and background models are consistent with the double-difference solution. Details are provided in Table 4. The COM clock products are distributed together with the COM orbit products. Based on the reprocessed COM orbits mentioned in Sect. 3.1, consistent sets of clock products (including GLONASS) were generated for the entire year 2014.

Table 4 Specifications of the COM clock processing

GNSS considered	See Table 3
Processing mode	See Table 3
Time span	Since DOY 288/2012 (GPSWEEK 1710)
Processing scheme	Zero-difference processing (observable: undifferenced code and phase, ionosphere-free linear combination)
Signals used	See column "Use" in Table 1
Obs. sampling	300 s
Elevation mask	5°; elev.-dependent weighting ($\cos^2(z)$)
Antenna info	See Table 3
Attitude model	See Table 3
A priori info	Orbits, ERPs, coordinates, and troposphere introduced from COM orbit solution
Product list	Epoch-wise (300 s) satellite and station clocks stored in daily clock RINEX and SP3 files; daily ISBs for mixed stations, IFBs for GPS+GLONASS stations, and GPS P1-C1 DCBs in Bernese DCB and BIAS-SINEX formats
Distribution	See Table 3

4 Orbit and clock validation

The reprocessed sets of COM orbits (see Sect. 3.1) and satellite clocks (see Sect. 3.2) from 2014, based on the ECOM1 and ECOM2 SRP models, respectively, are validated and compared in Sects. 4.1 and 4.2. The focus is on assessing the overall performance of our current COM products for the different GNSS, on identifying issues demanding improvements, and on assessing the impact of the SRP model change from ECOM1 to ECOM2. The comparison of Galileo IOV and FOC orbits in Sect. 4.3 and the comparison with external orbit products in Sect. 4.4 are performed with products from 2015. In Sect. 4.5, we assess the detectability of satellite maneuvers for the new systems.

4.1 Validation of COM satellite orbits from 2014

Orbit misclosures

We compute orbit differences (misclosures) at the day boundaries between consecutive arcs in the inertial frame, which should be zero. The COM orbit product is extracted from the middle day of a 3-day-long arc solution (as described and evaluated by Lutz et al. (2016), for GPS and GLONASS satellites). This configuration contains to a certain extent a continuity condition between the orbits of consecutive days. Nevertheless, the internal consistency of the orbit product can be evaluated by this method separately for the along-track, cross-track, and radial components. Figure 3 illustrates the overall statistics of the COM orbit misclosures based on all midnight epochs of 2014. Satellites in eclipse or oriented in orbit normal mode are not considered in the statistics.

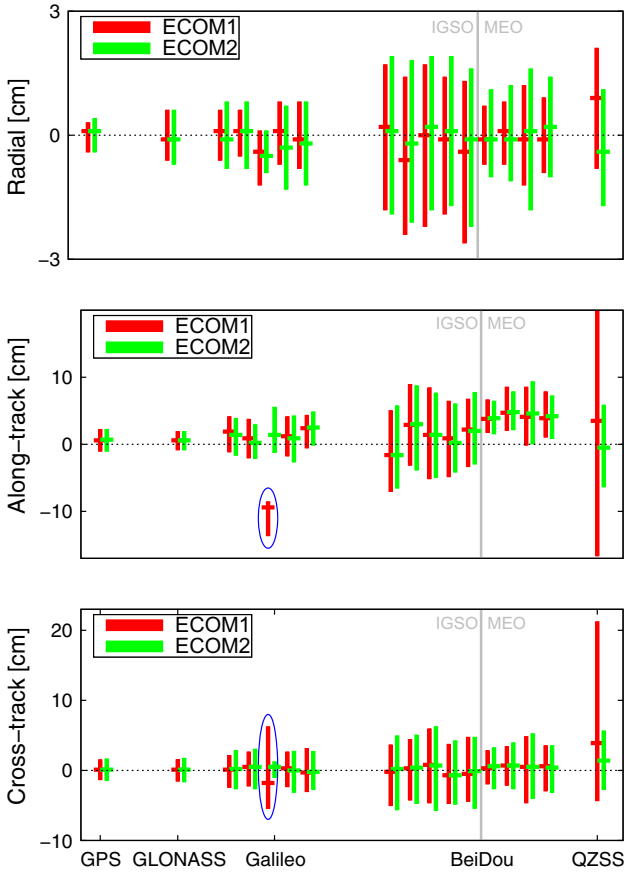

Fig. 3 Median (*horizontal bars*) and IQR (*vertical bars*) of the orbit misclosures for COM orbits of 2014 based on the ECOM1 or ECOM2 SRP models, respectively. GPS and GLONASS: system-wise. Other systems: satellite-wise with PRNs increasing from *left* to *right*. Note the different scales of the orbit components

The interquartile range (IQR) of the GPS and GLONASS orbit misclosures does not exceed 3.3 cm in any orbit component. The misclosures are minimally increased, if ECOM2 is used instead of ECOM1. In along-track, both GNSS have a median offset of about 0.6 cm. The Galileo IOV satellites have an IQR of up to 6 cm and a median offset of up to 2.5 cm in their largest (along-track) component. With ECOM2, the orbit misclosures are more noisy than with ECOM1—especially in the radial direction. The only FOC satellite in Fig. 3 (PRN E18) has—compared to other Galileo satellites—a larger IQR in cross-track (11.6 vs. 4.9 cm) and a significant offset in the along-track direction (−9.4 cm) when using ECOM1 (marked with blue ellipses in Fig. 3). With ECOM2, E18 is on a similar level as the IOV satellites. This issue is discussed in more detail in Sect. 4.3. Other pronounced characteristics in Fig. 3 are the large along- and

cross-track IQRs (36.5 and 25.5 cm) and significant offsets in all orbit components for the ECOM1-based solution of QZS-1 (PRN J01). With ECOM2, the IQR is reduced to a size comparable to that of the BeiDou IGSOs (≈12 and 8.3 cm in along- and cross-track). The offsets are significantly reduced, too. Most BeiDou satellites show an offset (up to 3 cm for the IGSOs and ≈5 cm for the MEOs) in the along-track orbit misclosures in Fig. 3. These offsets do not change with the new SRP model. The IQRs reach values of up to ≈13.5 cm for the IGSO and ≈9 cm for the MEO satellites in along-track. With ECOM2, the orbit misclosures are more noisy than with ECOM1—especially in the radial direction.

SLR residuals

The COM orbits of 2014 were also validated with Satellite Laser Ranging (SLR). This technique measures the distance between an SLR observatory and a satellite equipped with a laser retro-reflector array (LRA) from the measured light propagation time and the known speed of light. SLR residuals are the differences between observed (using SLR) and computed (based on the satellite orbits and the station coordinates in the SLRF2008 reference frame) distances at the measurement epochs. They allow for an independent validation of GNSS satellite orbits—at the typical orbit height of GNSS satellites mainly of the radial orbit component (Sośnica et al. 2015). While only two GPS satellites (SVNs G035 and G036) had reflectors, all GLONASS, Galileo, BeiDou, and QZSS satellites carry LRAs. Among the BeiDou satellites, only the PRNs C01 (GEO), C08, C10 (both IGSO), and C11 (MEO) were observed by the International Laser Ranging Service (ILRS, Pearlman et al. 2002) in 2014. In this work, the LRA offsets as recommended by the ILRS are used (see ILRS 2015).

Figure 4 shows the median offset and the IQR of the SLR residuals related to the COM orbits of 2014. Residuals of satellites in eclipse season or oriented with orbit normal attitude are excluded from the statistics. For the GPS satellite SVN G036, the median SLR offset and IQR are reduced when switching from the ECOM1 to the ECOM2 SRP model (offset: −1.9 to −1.1 cm; IQR: 4.3 to 3.2 cm).

For GLONASS, we identify two groups of satellites behaving in a different way in our SLR analysis (see Table 5). Satellites of group 1 behave as reported by Arnold et al. (2015): the median SLR offset and the IQR are reduced when using ECOM2 instead of ECOM1. Group 2 has a larger IQR, which is mainly caused by R09 in case of using ECOM1. With ECOM2, the median SLR offset and IQR are significantly larger for this group. This increase was not reported by Arnold et al. (2015) in their analysis of GLONASS orbits of 2012 and 2013. The authors stated, however, that they excluded satellites R11/SVN R723 and R21/SVN R725 (both assigned to group 2 in Table 5) as outliers from their SLR validation, because their SLR residuals looked peculiar and became larger when ECOM2 was applied.

For GLONASS satellites of group 1, such as R24 (see Fig. 5, top), the β-dependent and the Δu (argument of

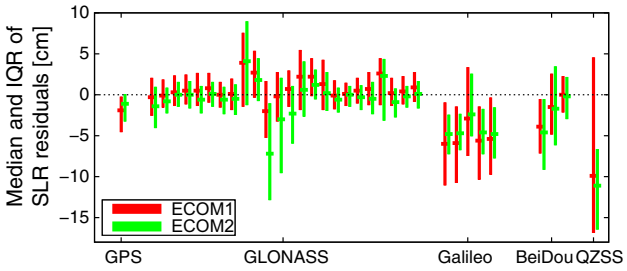

Fig. 4 Median offset (*horizontal bars*) and IQR (*vertical bars*) of the SLR residuals of COM orbits of 2014 based on the ECOM1 or ECOM2 SRP models, respectively. Satellite PRNs are increasing from *left* to *right*

Table 5 SLR residual statistics of 2014 for two groups of GLONASS satellite vehicles (SV) when using ECOM1 (E1) and ECOM2 (E2). Note that SVN R755 replaced SVN R725 as slot number R21 on 02 Aug 2014

Group	Slot-number	SVN	Median (cm)		IQR (cm)	
			E1	E2	E1	E2
1	All SV not in group 2		0.5	−0.2	3.8	3.3
	plus R21	755				
2	R01, R09,	730, 736,	0.5	−1.3	6.6	10.5
	R11, R12,	723, 737,				
	R13, R21,	721, 725,				
3	All GLONASS satellites		0.5	−0.3	4.4	4.2

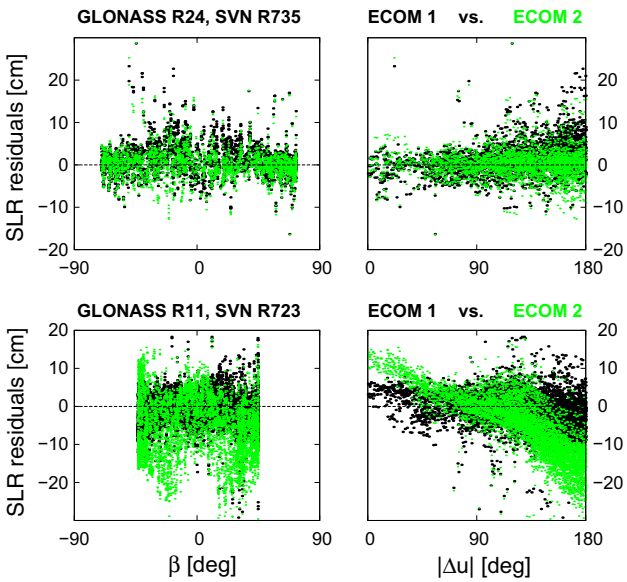

Fig. 5 SLR residuals of GLONASS satellites from 2014 as a function of the β-angle (*left*) and the argument of latitude Δu (*right*). *Top* R24 (group 1). *Bottom* R11 (group 2)

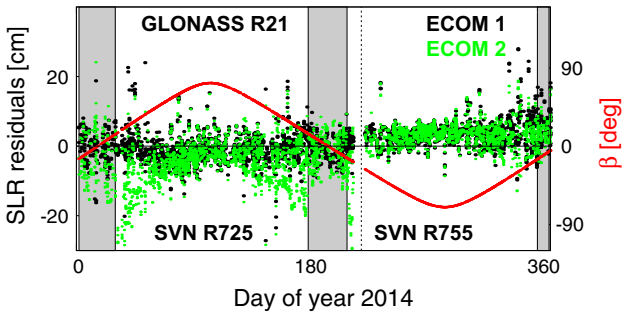

Fig. 6 SLR residuals of GLONASS R21 as a function of time. SVN R725 was replaced by SVN R755 on 02 Aug 2014. *Gray* eclipse seasons. *Red* β angle

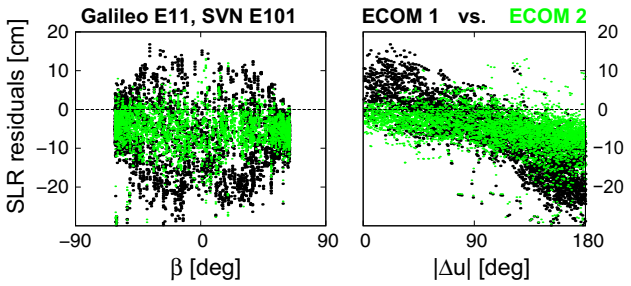

Fig. 7 SLR residuals of Galileo E11 from 2014 as a function of the β-angle (*left*) and the argument of latitude Δu (*right*)

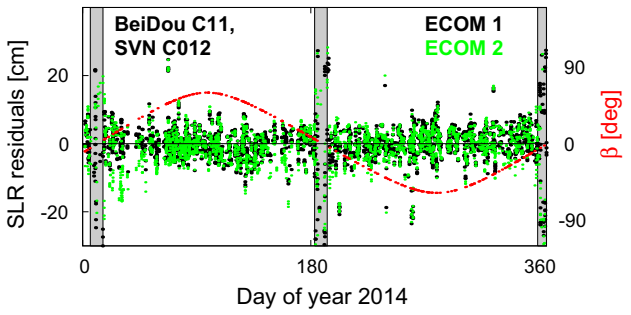

Fig. 8 SLR residuals of BeiDou C11 (MEO) as a function of time. *Gray* orbit normal mode. *Red* β angle

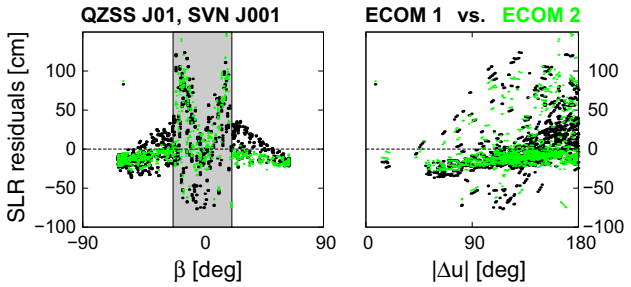

Fig. 9 SLR residuals of QZS-1 from 2014 as a function of the β angle (*left*) and the argument of latitude Δu (*right*). *Gray* orbit normal mode

latitude)-dependent systematics are reduced when replacing ECOM1 by ECOM2. For satellites of GLONASS group 2, such as R11 (see Fig. 5, bottom), however, these systematics grow considerably. The example of GLONASS R21 in Fig. 6 shows that the effect must be related to the individual spacecraft: in early 2014, this slot number was assigned to the old satellite SVN R725, belonging to group 2 in Table 5. Later in 2014, R21 was assigned to the new satellite SVN R755, which belongs to group 1. The SLR residuals of satellites of group 2 are largest just before and after the eclipse seasons. Interestingly, the number of satellites that have to be assigned to group 2 increased from 2 in 2012–2013 (Arnold et al. 2015) to 6 in 2014 (Table 5). The majority of them populate the second orbital plane of GLONASS. The satellites on this plane generally show a larger IQR in Fig. 4 than the satellites on the other two planes.

For Galileo, we see a clear improvement of the SLR residuals when using ECOM2: the median SLR offset is reduced from −5.8 to −4.7 cm, the IQR from 9.3 to 4.9 cm. Figure 7 shows the example of PRN E11. The β-dependent and the Δu-dependent systematics are clearly reduced, but not completely eliminated. These results are representative for all Galileo satellites.

For BeiDou satellites, the SLR residual statistics in Fig. 4 show different offsets (0 to −3.9 cm in the case of ECOM1) and IQRs (4.3 to 7.3 cm). The smallest offset and IQR can be assigned to the MEO satellite PRN C11. With ECOM2, the SLR residuals are degraded—especially for the IGSO satellites. The time series of SLR residuals in Fig. 8 does not show a clear dependency on the β-angle. It shows, however, that the SLR residuals are increased when the satellites are in orbit normal mode.

QZS-1 has a significant offset and the largest IQR of all satellites with ECOM1 in Fig. 4. Replacing the ECOM1 with the ECOM2 significantly reduces the IQR from 21.3 to 9.7 cm. The SLR offset, however, increases from −9.9 to −11.1 cm. Figure 9 shows that these changes are attributed to the reduction of the Δu-dependent and the β-dependent systematics during times with yaw-steering attitude. Note that the SLR residuals are largest (>100 cm) at $\beta \approx \pm 20°$ (i.e., when QZS-1 switches between yaw-steering and orbit normal attitude modes) and smaller in the middle of the orbit normal mode interval (i.e., $\beta \approx 0°$) when the orbit normal mode is close to the yaw-steering assumed in our analysis.

4.2 Validation of COM satellite clocks of 2014

Assuming that the epoch-specific satellite clock corrections of highly stable clocks may be represented over one day by a linear function, the RMS error of the fit may serve as a quality indicator. If computed independently for each day (i.e., independent from day-to-day changes of the selected clock reference and ISB), the time series of daily clock RMS values is suitable for the long-time monitoring of the clock performance. A large RMS of the linear approximation may be caused by a low stability of the clock, bias variations in

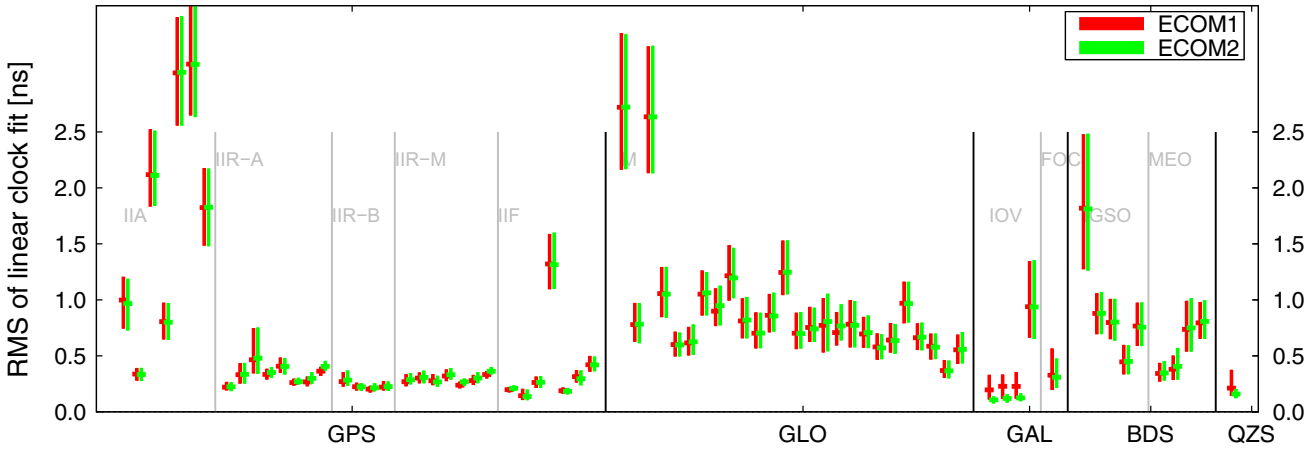

Fig. 10 Median (*horizontal bars*) and IQR (*vertical bars*) of the daily RMS of linear clock fit for COM clocks of 2014 when using the ECOM1 or ECOM2 SRP models, respectively. GNSS are separated by *vertical black lines*. Blocks are separated by *vertical gray lines*. Satellite SVNs are increasing from *left* to *right* within each block

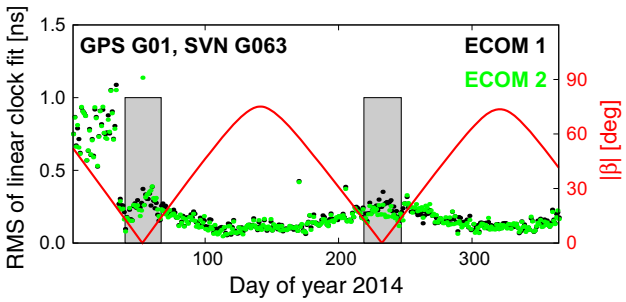

Fig. 11 RMS of linear fit through clock corrections of GPS G01/SVN G063 (Block IIF) based on the ECOM1 or ECOM2 SRP models, respectively. *Gray* eclipse seasons. *Red* absolute value of β

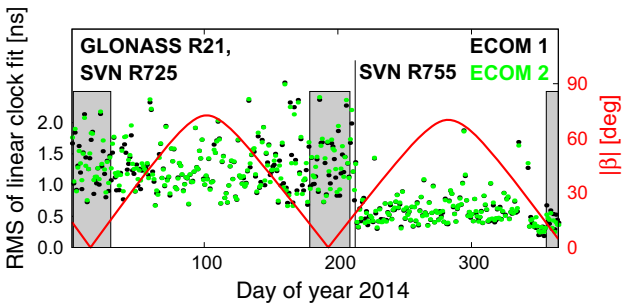

Fig. 12 RMS of linear fit through clock corrections of GLONASS R21 based on the ECOM1 or ECOM2 SRP models, respectively. *Gray* eclipse seasons. *Red* absolute value of β

the transmitter chain (Montenbruck et al. 2012), or by orbit (or other) errors, which are mapped into the satellite clocks in the parameter estimation process. Thus, stable satellite clocks are in principle suitable for the validation of the radial orbit component. A precondition is that always a stable clock is selected as clock reference. Figure 10 gives an overview of the clock RMS statistics for all satellites in the COM solution of 2014. For BeiDou and QZSS satellites, time intervals with orbit normal attitude are excluded from the statistics.

The performance of GPS satellite clocks depends on the satellite type. The clocks of GPS Block IIA satellites generally show the poorest performance with a median RMS of up to 3 ns. SVN G026 is exceptionally good. Most Block IIR clocks are more stable than Block IIA clocks (median RMS below 0.4 ns and IQR about 0.1 ns). The values are similar for the Block IIF satellites, except for G24/SVN G065, which is running on a cesium clock instead of an RAFS clock (Langley 2016). The clock performance may vary over time (e.g., after a clock switch or reset). G01/SVN G063, for example, had a poor clock performance in early 2014, but became excellent after DOY 34/2014 (see Fig. 11). Even though the clocks of most Block IIR and IIF satellites are stable enough for orbit validation, their statistics in Fig. 10 do not depend on the ECOM version. The time series in Fig. 11 does also show only minimal differences between the ECOM1- and ECOM2-based solutions during the eclipse seasons. The small β-angle-dependent signal in Fig. 11 might partly be related to thermal effects affecting the stability of the satellite clock and the biases (Montenbruck et al. 2012).

Figure 10 shows that the performance of most GLONASS-M satellite clocks is worse than that of typical GPS Block IIR and IIF clocks expressed by the median RMS (≈0.5 to 3 ns) and IQR (≈0.2 to 1 ns). (located more on the right-hand side in Fig. 10) tend to have smaller median RMS values than the older ones. We do not see a clear dependency on the β angle or on the SRP model in the GLONASS clock RMS. Figure 12 shows a minimal degradation of the clock RMS during and close to the eclipse seasons of SVN R725, when replacing ECOM1 by ECOM2. From the orbit validation in Sect. 4.1, we know, however, that the orbit of this satellite is significantly degraded at the same time periods when using ECOM2 (Fig. 6). Obviously, orbit errors and attitude mismodelings are not the main error source affecting GLONASS satellite clock corrections. The RMS of the linear clock fit at this

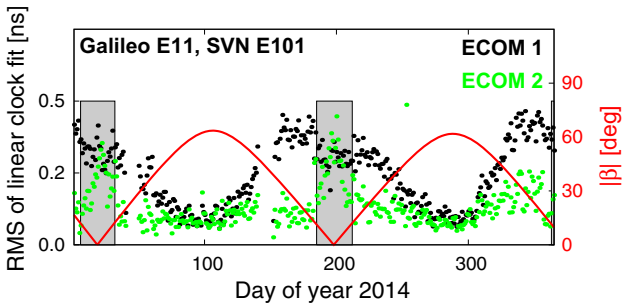

Fig. 13 RMS of linear fit of Galileo E11 clocks when using the ECOM1 and ECOM2 SRP models, respectively. *Gray* eclipse seasons. *Red* absolute value of β

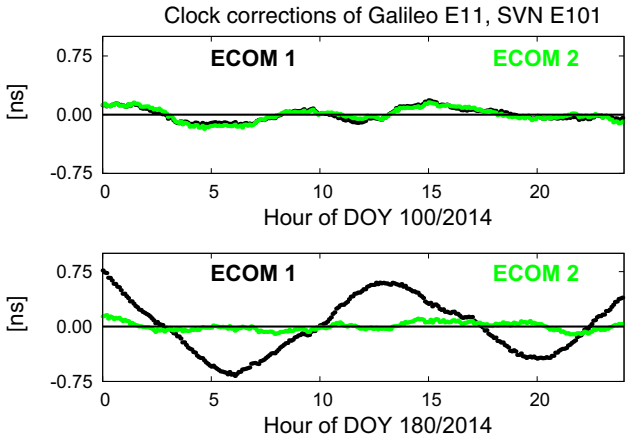

Fig. 14 Satellite clock corrections of Galileo E11 when using the ECOM1 and ECOM2 SRP models, respectively. *Top* DOY 100/2014. *Bottom* DOY 180/2014

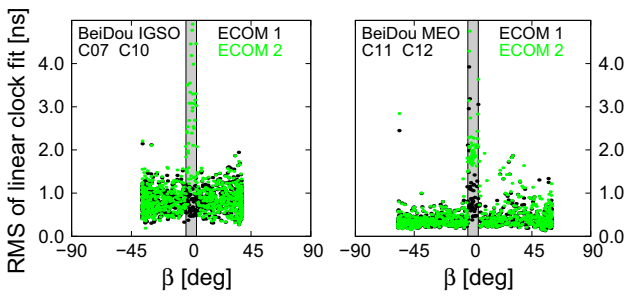

Fig. 15 RMS of linear fit as a function of the β angle for BeiDou satellite clocks from 2014 based on the ECOM1 and ECOM2 SRP models, respectively. *Left* IGSOs C07 and C10. *Right* MEOs C11 and C12. *Gray* orbit normal mode

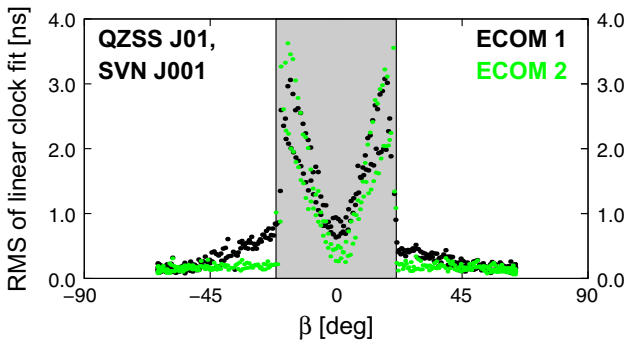

Fig. 16 RMS of linear fit as a function of the β angle for the QZS-1 satellite clocks of 2014 based on the ECOM1 and ECOM2 SRP models, respectively. *Gray* orbit normal mode

level (0.5 ns and larger) is rather dominated by the clock noise.

The statistical properties of the Galileo clocks in Fig. 10 are comparable with those of GPS Blocks IIR and IIF. An exception is E20, with a clock performance comparable to GLONASS. On E20, a RAFS clock was active in 2014, while PHM clocks were active on the other Galileo IOV satellites (see also Sect. 2). For satellites running on PHMs, the median RMS and IQR improve if ECOM1 is replaced by ECOM2. The time series of the clock RMS in Fig. 13 shows that this is due to a significant reduction of the β-dependent signal. The close agreement with the results of the SLR orbit validation in Sect. 4.1 suggests that a significant part of the clock errors is orbit-induced. This assumption is confirmed by the clock time series of Galileo E11 from DOY 180/2014 showing that the large RMS, the ECOM1-based solution has at this day, is due to a (1/rev) signal with an amplitude of about 0.7 ns (Fig. 14, bottom). The clock solution related to the ECOM2-based orbits does not show this signal, because the ECOM2 is able to absorb most of the SRP signal in the orbits. Figure 14 (top) shows that the clock estimates of E11 are not affected by the (1/rev) signal on DOY 100/2014, because the β angle is large and consequently the illuminated cross-section of the satellite body does not vary much (i.e., the ECOM1 works sufficiently well in this scenario). During the eclipse seasons, the RMS of the clock corrections remains large and can even increase when changing from ECOM1 to ECOM2 (see Fig. 13). This increase is likely caused by the Galileo attitude behavior at small β angles, which is not yet correctly considered in the COM solution. Similar to GLONASS, the change of the SRP model has no impact on the clocks of E20, despite the fact that its orbit benefits from the model change in the same way as those of the other Galileo satellites. We conclude that the Galileo PHM clocks are well suited for orbit validation, while the RAFS clocks are not.

The clock performance of the BeiDou satellites is comparable to that of GLONASS in Fig. 10. The clock of C06 shows the poorest performance. In intervals with orbit normal mode, the clock RMS of BeiDou IGSO and MEO satellites degrades significantly when replacing ECOM1 by ECOM2 (Fig. 15). From the orbit validation we know that large orbit errors occur at these intervals (see Fig. 8). They are obviously mapped into the clocks. Apart from such big orbit errors, BeiDou clocks are too noisy to be used for orbit validation.

The median RMS and the IQR of the QZS-1 clock in Fig. 10 are at a similar level as the corresponding val-

Table 6 Median and IQR of orbit misclosures in the radial (R), along-track (A), and cross-track (O) directions and of SLR residuals (S) of the Galileo IOV and FOC1 (PRNs E14 and E18) satellites during the time interval DOY 01/2015–DOY 130/2015 when using the ECOM1 (E1) and ECOM2 (E2) SRP model (M)

M	Sat typ	Median [cm]				IQR [cm]			
		R	A	O	S	R	A	O	S
E1	IOV	0.1	-0.3	0.1	-6.5	3.8	11.7	9.8	8.9
E1	FOC	0.0	4.7	-0.3	-3.7	3.4	13.9	12.4	8.2
E2	IOV	-0.2	0.3	-0.4	-4.2	1.5	7.0	6.3	4.0
E2	FOC	0.1	2.6	0.6	-1.1	1.1	8.0	4.5	4.2

ues of the Galileo PHM satellite clocks. As in the case of Galileo, the clock statistics improve when replacing ECOM1 by ECOM2. The reason is that the β-dependent errors of the QZS-1 clock are significantly reduced during time periods with yaw-steering when using ECOM2 instead of ECOM1 (see Fig. 16). The clock RMS is, however, largest (up to 4 ns) during time periods with orbit normal mode (in particular at times close to the switch between yaw-steering and orbit normal attitude mode). This behavior agrees with the results of the SLR orbit validation in Sect. 4.1.

4.3 Orbit misclosures of the first Galileo FOC satellites

The orbit misclosures of the first active Galileo FOC satellite PRN E18 in Fig. 3 differ significantly from the values of the Galileo IOV satellites when using ECOM1 in the orbit determination: the offset is larger in the along-track component and the IQR in the cross-track component. However, the statistics shown in Fig. 3 are based on only 10 days of data available for E18 in 2014. Due to their eccentric orbits and stable PHM clocks (see Table 2), the first two Galileo FOC satellites are of interest not only for the Galileo constellation but also for research on relativistic effects (Delva et al. 2015). Therefore, we reprocessed orbits of the first 130 days of 2015 using the ECOM1 SRP model and compared them with the operational COM products (based on ECOM2 since early 2015).

The orbit misclosure statistics in Table 6 show similar systematics as Fig. 3, which is based on data of 2014: with ECOM1, the FOC1 satellites have a significant offset in the along-track misclosures. Their IQR is larger than that of the IOV satellites in along- and cross-track. With ECOM2, the along-track offset is reduced, though not disappeared. The IQR is significantly reduced for all Galileo satellites. For the FOC1 satellites, it is even smaller than for the IOV satellites in the radial and cross-track directions, while it is slightly larger in along-track.

The SLR residual statistics in Table 6 confirm the improvement of all Galileo orbits when changing from ECOM1 to ECOM2: the IQR is halved and has about the same size for both satellite types (≈4 cm with ECOM2). The median SLR offset is reduced, too. For the FOC1 satellites, it is even smaller than for the IOV satellites (−1.1 vs. −4.2 cm in the case of using ECOM2), which is in agreement with Fig. 4. These results show that the orbit accuracy of the Galileo FOC1 satellites is comparable with that of the IOV satellites in the COM solution using the ECOM2 SRP model.

Table 7 SLR residual statistics for MGEX orbits from different ACs. Time interval: second quarter of 2015 (DOYs 95-180/2015). In brackets: satellites with orbit normal mode are excluded

GNSS	AC	Median (cm)	IQR (cm)
GLONASS	COM	−0.1	3.9
	GBM	−0.3	5.9
	GRM	−1.0	6.0
	WUM	−0.3	5.9
Galileo	COM	−3.0	5.3
	GBM	−1.9	12.9
	GRM	1.0	7.6
	TUM	−3.2	14.3
	WUM	−2.4	5.9
BeiDou	COM	−2.0	7.6
		(−1.9)	(6.7)
	GBM	1.6	6.9
		(1.5)	(6.7)
	WUM	0.1	6.8
		(0.1)	(6.8)
QZSS	COM	−13.4	8.0
	GBM	−10.6	10.5
	QZF	−16.9	15.6
	TUM	−7.3	19.3
	WUM	−15.8	16.4

4.4 Comparison of the orbit accuracy with other MGEX solutions

We compare the SLR statistics of orbit products from ACs providing MGEX solutions in the second quarter of 2015. Apart from CODE (COM), the MGEX ACs at GFZ Potsdam (GBM), GRGS (GRM), the QZSS operations center (QZF), TU München (TUM), and Wuhan University (WUM) provide orbits in this time interval. The statistics are summarized in Table 7.

For GLONASS, the median SLR offset is close to zero and the IQR is ≈6 cm for most ACs. The COM solution benefits from the GLONASS ambiguity resolution resulting in a smaller IQR. The Galileo orbits of most ACs have a median offset with a size of about 2–3 cm and a negative sign. The GRM solution with an offset of +1 cm is an exception. The IQR differs for the ACs: for COM and WUM, it is ≈5–6 cm; for GBM and TUM, it is ≈13–14.5 cm; and for GRM, it is ≈7.5 cm. When compared by Steigenberger et al. (2015), the Galileo orbits of COM and TUM

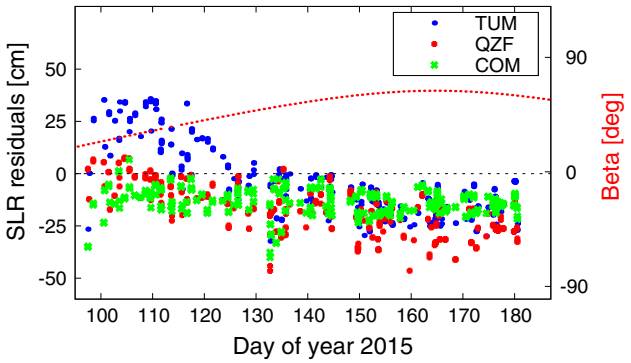

Fig. 17 SLR residuals of QZS-1 orbits from different MGEX ACs during the time interval DOY 95/2015–DOY 180/2015. *Red* β-angle

from 2013 (both using the ECOM1 SRP model at that time) were comparable in quality. The COM solution of 2015, however, benefits from the ECOM2 model (see Sects. 4.1 and 4.3), while GBM and TUM still use the ECOM1. The WUM and GRM solutions perform relatively well, because they use advanced SRP models for Galileo, as well (see Guo et al. 2016; Steigenberger et al. 2015). The SLR residuals of the COM and GBM BeiDou orbits show a median offset with a different sign, respectively. For WUM, however, the median is almost 0 cm. If satellites in orbit normal mode (concerning PRNs C08 and C11 within the selected time interval) are excluded, the IQR of all solutions is below 7 cm. If these satellites are included, the IQR is significantly larger for COM, but not for GBM (Deng et al. 2016) and WUM (Guo et al. 2016) as these solutions consider the orbit normal mode.

QZS-1 was in the yaw-steering mode during the whole time interval DOY 95/2015–DOY 180/2015 (it switched back to yaw-steering just before the beginning of the interval). QZS-1 orbits are provided by COM, QZF, and TUM for the entire time interval, whereas GBM and WUM provide them only from DOY 147/2015 on. Figure 17 shows the SLR residuals of QZS-1 for the "complete" solutions. The QZS-1 orbits of all ACs have a significant SLR offset with negative sign and sizes between ≈7.5 and ≈17 cm (Table 7). The TUM solution has the largest IQR (≈19 cm). Similar to the COM solution of 2014 based on the ECOM1 SRP model (see Fig. 9), the SLR residuals change with the β-angle, resulting in a wide range of residual values (with positive and negative signs) within the time interval. This explains the big IQR and the small offset (−7.3 cm) of this solution. The COM solution shows a similar behavior as the reprocessed, ECOM2-based solution from 2014 in Fig. 9: the correlation with the β angle is relatively small, explaining the comparatively small IQR (≈8 cm) and the relatively constant offset (≈−13.5 cm). The QZF solution shows a moderate dependency on the β angle. The IQR (≈15.5 cm) is between that of the TUM and COM solutions. This can be explained by the use of an SRP model that considers the shape of the satellite body (Steigenberger and Kogure 2014). As the GBM and WUM solutions are only available from DOY 147/2015 on, their statistics in Table 7 are hardly affected by the changing β-angle. Therefore, their IQRs have moderate values of ≈10.5 and ≈16.5 cm, respectively.

4.5 Satellite repositioning events

In the classical IGS processing satellite, maneuvers had to be handled mainly for GPS satellites (about once per year per satellite). The inclusion of BeiDou since late 2013 and QZSS since early 2014 in the COM solution offered the opportunity to apply a repositioning detection procedure similar to the one used for CODE's IGS processing (Dach et al. 2009) on the new GNSS: for a repositioned satellite, the orbit arcs before and after the repositioning event are both extrapolated to the day of the assumed maneuver and compared. The epoch of closest approach of the overlapping orbital arcs is assumed to be the maneuver time. The velocity difference at this time is taken as the velocity change.

For detected repositionings, estimated maneuver times and velocity changes in the radial, along-track, and cross-track components are listed in Table 8. Regular (about every half year) repositionings were detected for all IGSO satellites (BeiDou PRNs C06–C10 and QZS-1/PRN J01). As reported by Dach et al. (2009), the velocity changes occur mainly in along-track direction for GPS repositionings. For most repositionings of BeiDou IGSO satellites, however, a significant velocity change was also observed in the cross-track component. This confirms results recently presented by Qiao and Chen (2015). While BeiDou repositionings can be detected with the described algorithm without problems, we were not able to assign unambiguous repositioning times for QZS-1. The QZS-1 values in Table 8 are, therefore, only rough approximations. We did not find repositionings for the Galileo and BeiDou MEO satellites.

5 Summary and discussion

In Sects. 2, 3.1, and 3.2, we demonstrated that the integration of new GNSS (Galileo, BeiDou, and QZSS) and (RINEX3) data into our existing processing schemes is possible: we are now able to generate orbits and clock corrections for these systems on a routinely basis. Satellite maneuvers can be handled, as well (Sect. 4.5). In this first step, we, however, had to make compromises and simplifications regarding processing standards and background models. The results of the orbit validation in Sect. 4 show that these compromises have an impact on the orbit accuracy of the new systems. Compared with GPS and GLONASS, their orbit misclosures

Table 8 Detected BeiDou and QZS-1 repositionings with velocity changes in radial, along-track, and cross-track components

PRN	Date	Time	Velocity change (mm/s)		
			Radial	Along	Cross
C06	2014-05-08	22:40:30	5.2	−592.5	−339.4
C06	2014-11-03	08:35:28	−0.6	−604.7	−233.9
C06	2015-05-10	22:35:18	4.2	−593.6	−411.4
C07	2013-11-29	11:00:28	0.8	−575.0	368.3
C07	2014-05-23	00:30:06	7.5	−588.8	445.8
C07	2014-11-25	09:30:25	0.7	−599.4	395.6
C07	2015-05-28	00:30:15	6.4	−609.8	412.4
C08	2013-12-26	13:10:25	−0.4	−585.4	−63.2
C08	2014-07-11	09:20:28	−0.7	−614.2	−92.6
C08	2015-01-09	14:00:39	0.2	−579.9	134.8
C08	2015-07-26	09:35:21	−0.1	−610.5	−258.1
C09	2014-03-26	00:40:04	7.1	−389.0	117.1
C09	2014-09-22	08:40:24	0.4	−367.9	278.8
C09	2015-03-31	00:35:10	6.8	−400.8	66.4
C10	2014-01-10	08:40:24	−0.0	−351.6	106.0
C10	2014-07-01	00:29:55	4.1	−358.0	105.6
C10	2014-12-22	08:00:24	−0.1	−360.4	251.6
C10	2015-06-18	22:40:33	2.9	−380.7	150.7
J01	2014-04-30	**09:15–17:45**			
J01	2014-10-29-	**19:30-**			
	2014-10-30	**04:00**			
J01	2015-04-22	**07:00–20:30**			

Bold: QZS-1 repositioning times are rough estimates

are larger and have an offset in the along-track component (see Fig. 3). The SLR residuals have an offset for most of the new satellites, as well (see Fig. 4). Both offsets can be attributed to modelling deficiencies with impact in the radial direction, i.e., on the determination of the satellite's semimajor axis defining the orbit scale and the revolution period. This concerns models for the receiver and transmitter antenna phase center (see, e.g., Dilssner et al. 2014), the Earth re-radiation, and the transmitter antenna thrust (Rodriguez-Solano et al. 2012). As stated in Sect. 3.1, these models are not or not yet sufficiently implemented for the new GNSS in the COM solution. The missing integer ambiguity resolution and the sparser tracking network (see Sect. 2) contribute to the poorer overall performance of the new systems, as well.

Section 4 shows that the orbit errors are larger for the IGSO satellites than for the MEO satellites—although they are treated in the same way. Possible reasons are the longer revolution period and the different observation geometry of IGSO satellites. The impact of the orbit arc-length on the estimation of orbit and reference frame parameters was thoroughly evaluated by Lutz et al. (2016) for GPS and GLONASS. Similar investigations of the optimal arc-length and orbit model are also necessary for IGSO and GEO satellites, as their orbits are different regarding revolution time, observation geometry, inclination, and eccentricity (in the case of QZSS). For GEO satellites, the observation geometry is not changing at all, which is another challenge (especially for ambiguity resolution). In this context, it could be worth to assess the possible contribution of IGSO and GEO satellites to IGS products.

The misclosures of the ECOM1-based Galileo FOC1 orbits shown in Sects. 4.1 and 4.3 indicate that the orbit eccentricity might have an impact on the orbit determination, as well. For satellites with eccentric orbits (e.g., Galileo FOC1 and QZSS), the implications on orbit integration, background models (e.g., SRP model), arc-length, and optimal sampling rate of the orbit files (e.g., SP3 format) are not yet sufficiently investigated.

The SLR orbit validation (see Sect. 4.1) and the clock validation (see Sect. 4.2) show that the SRP modelling is more challenging with the increased variety of GNSS design specifications involved in a multi-GNSS analysis. While the ECOM1 SRP model is sufficient for GPS and BeiDou, it shows deficiencies for satellites with elongated bodies, namely GLONASS, Galileo, and QZSS. We demonstrate that ECOM2 significantly improves the orbit determination of Galileo and QZSS during yaw-steering by removing a (1/rev) signal. For the majority of the GLONASS satellites, we confirm the moderate reduction of the SLR residuals seen by Arnold et al. (2015). We see, however, a significant degradation for a growing number of GLONASS satellites. These results show that the increased number of estimation parameters in ECOM2 compared with ECOM1 improves the modelling capabilities. On the other hand, they indicate that the solution might be less stable and more sensitive to other modelling errors (e.g., attitude). Both the stability of empirical SRP models and the unexpected side-effects on GLONASS POD demand further investigations.

As mentioned in Sect. 3.1, the correct attitude laws for midnight and noon turns during eclipse seasons (in the case of GPS, GLONASS, and Galileo) or for orbit normal mode phases (in case of BeiDou and QZSS) are not yet implemented in the COM solution. The larger RMS of the Galileo clock corrections during the eclipse seasons (visible for the ECOM2-based solution in Fig. 13, but also in SLR residuals) could possibly be attributed to this. Even larger (>100 cm) orbit errors occur for BeiDou and QZSS satellites during periods, when these satellites are in the orbit normal mode (see Figs. 8, 9). These orbit errors are mapped into the satellite clock corrections (see Figs. 15 and 16) and might even affect common parameters (such as station coordinates) in the integrated processing approach used to generate the COM solution. We, therefore, consider the implementation

of the orbit normal mode for BeiDou and QZSS satellites as mandatory. This, in return, requires adaptations of the SRP modelling, because the existing ECOM models are strictly designed for yaw-steering (Arnold et al. 2015).

As stated in Sect. 2 and in Sect. 3, observation biases are treated in a simplified way in the COM solution. The estimated ISBs are provided as frequency-specific quantities. The underlying signal types (e.g., C1C and C1X) are not specified. It is possible that the ambiguous definition of the reference signals and ISBs might cause problems for the combination of clocks from different ACs. The correct setup, bookkeeping, and reporting of the observation biases are, therefore, challenges, the IGS has to solve before the new systems can fully contribute to all of its products. Alternatively, the signal selection might be restricted by convention. Nethertheless, the clock validation in Sect. 4.2 illustrates the large performance differences of clocks used in different types of GNSS satellites. It is demonstrated that the best satellite clocks available today are even suited for orbit validation. Galileo PHM, QZSS, and most GPS Block IIR and IIF clocks belong into this category.

In Sect. 4.4, we demonstrate that the COM orbits are, in spite of their above-mentioned deficiencies, comparable in quality to other MGEX solutions. The comparison shows that the ACs have different priorities in solving the open issues. Section 4.4 suggests that—thanks to the ECOM2—our strengths are currently in the Galileo and QZSS orbit determination at yaw-steering. A COM-specific weakness is the attitude modelling—especially during the orbit normal mode. Other issues, such as the missing or insufficient implementation of antenna calibrations, albedo models, and transmitter antenna thrust, currently seem to affect most MGEX ACs.

6 Conclusions

The goal of the MGEX is to pave the way for the inclusion of new satellite systems and observation data stored in RINEX3 files into the operational IGS products (Montenbruck et al. 2013). In the previous sections, we presented the data basis, processing strategy, and results of the CODE AC contribution to MGEX. We pointed out that, in the first phase of MGEX, our priority was on the extension of our processing schemes to support the new systems and data. The discussion in Sect. 5 shows that the final goal of MGEX is not yet achieved—provided that the new systems shall contribute to IGS products to the same extent as GPS and GLONASS. The current COM solution is, however, the baseline for the necessary improvements and adaptations. The analysis of our preliminary results identified that the following issues need to be improved w.r.t. the new GNSS:

- Receiver and transmitter antenna PCO + PCV
- Earth radiation (albedo) pressure model
- Transmitter antenna thrust model
- Integer ambiguity resolution
- Orbit normal mode attitude (BeiDou, QZSS)
- SRP model for orbit normal mode (BeiDou, QZSS)

Other challenges arise from the increased variety of frequencies and signals available with the new RINEX3 data format. They concern established and new systems alike and deserve further research:

- Optimal frequency- and signal-selection
- Bookkeeping of selected observation types
- New linear combinations?
- Bookkeeping, provision, and application of biases for code and phase observations

More challenges arise from the fact that different GNSS and orbit types are combined in a multi-GNSS environment:

- Optimal station selection and network configuration considering the different orbit types and the presence of RNSS
- Handling of intersystem biases for common parameters, such as receiver clocks, coordinates, troposphere, and ERPs
- Optimal arc-length (common or orbit type specific?)

In Sects. 2 and 3, we stated that many of the above-mentioned issues are not yet (e.g., implementation of orbit normal mode), not completely (e.g., receiver and transmitter antenna model), or not yet optimally (e.g., observation type selection) solved for the COM solution. The comparison with orbits provided by other ACs in Sect. 4.4 shows that they are in a similar situation. As confirmed by the orbit and clock validation in Sect. 4, we achieved a significant improvement regarding the SRP modelling of Galileo and QZSS during yaw-steering by replacing the ECOM1 SRP model by ECOM2.

We conclude that multi-GNSS orbit and clock determination remain challenging. Many questions are not yet answered. We plan to improve the COM solution step-by-step by correcting the deficiencies identified in this work. The IGS MGEX proved to be a suitable testbed for this task. We will need it also in the near future to identify challenges, derive models (e.g., satellite antenna models), and validate the impact of processing- and model-improvements. More information about satellite properties will be needed, as well.

Acknowledgements We thank all institutions providing and distributing raw data of MGEX stations. We thank the ILRS for providing SLR

measurements to a variety of GNSS satellites which are valuable for an independent orbit validation.

References

Arnold D, Meindl M, Beutler G, Dach R, Schaer S, Lutz S, Prange L, Sośnica K, Mervart L, Jäggi A (2015) CODEs new solar radiation pressure model for GNSS orbit determination. J Geod 89(8):775–791. doi:10.1007/s00190-015-0814-4

Bar-Sever YE (1996) A new model for GPS yaw attitude. J Geod 70(11):714–723. doi:10.1007/BF00867149

Beutler G, Brockmann E, Gurtner W, Hugentobler U, Mervart L, Rothacher M (1994) Extended orbit modeling techniques at the CODE processing center of the international GPS service for geodynamics (IGS): theory and initial results. Manuscr Geod 19:367–386

Bruyninx C, Baire Q, Legrand J, Roosbeek F (2011) The EUREF Permanent Network (EPN): Recent Developments and Key Issues. Presentation, EUREF 2011 Symposium, Chisinau, Republic of Moldova

Dach R, Brockmann E, Schaer S, Beutler G, Meindl M, Prange L, Bock H, Jäggi A, Ostini L (2009) GNSS processing at CODE: status report. J Geod 83(3–4):353–366. doi:10.1007/s00190-008-0281-2

Dach R, Schaer S, Lutz S, Meindl M, Bock H, Orliac E, Prange L, Thaller D, Mervart L, Jäggi A, Beutler G, Brockmann E, Ineichen D, Wiget A, Weber G, Habrich H, Ihde J, Steigenberger P, Hugentobler U (2012) Center for Orbit Determination in Europe: IGS technical report 2011. International GNSS Service: Technical Report 2011, edited by Meindl M, Dach R, and Jean Y (AIUB), IGS Central Bureau, pp 29–40. doi:10.7892/boris.80302

Dach R, Schaer S, Lutz S, Arnold D, Bock H, Orliac E, Prange L, Villiger A, Mervart L, Jäggi A, Beutler G, Brockmann E, Ineichen D, Wiget A, Rülke A, Thaller D, Habrich H, Söhne W, Ihde J, Steigenberger P, Hugentobler U (2015) CODE Analysis Center Technical Report 2014. International GNSS Service: Technical Report 2014, edited by Dach R and Jean Y (AIUB), IGS Central Bureau, pp 21–34. doi:10.7892/boris.80306

Dach R, Lutz S, Walser P, Fridez P (Eds) (2015) Bernese GNSS Software Version 5.2. User manual. Astronomical Institute, Universtiy of Bern, Bern Open Publishing. doi:10.7892/boris.72297

Dai X, Ge M, Lou Y, Shi C, Wickert J, Schuh H (2015) Estimating the yaw-attitude of BDS IGSO and MEO satellites. J Geod 89(10):1005–1018. doi:10.1007/s00190-015-0829-x

Delva P, Hees A, Bertone S, Richard E, Wolf P (2015) Test of the gravitational redshift with stable clocks in eccentric orbits: application to Galileo satellites 5 and 6. Class Quantum Gravity 32(23). doi:10.1088/0264-9381/32/23/232003

Deng Z, Fritsche M, Uhlemann M, Wickert J, Schuh H (2016) Reprocessing of GFZ Multi-GNSS product GBM. Presentation, IGS Workshop 2016, Sydney Australia, 08-12 Feb 2016

Dilssner F, Springer T, Gienger G, Dow J (2011) The GLONASS-M satellite yaw-attitude model. Adv Space Res 47(1):160–171. doi:10.1016/j.asr.2010.09.007

Dilssner F, Springer T, Schönemann E, Enderle W (2014) Estimation of satellite antenna phase center corrections for BeiDou. Poster, IGS Workshop 2014, Pasadena, USA, June 23-27 2014

Dow JM, Neilan RE, Rizos C (2009) The International GNSS Service in a changing landscape of Global Navigation Satellite Systems. J Geod 83(3–4):191–198. doi:10.1007/s00190-008-0300-3

European Space Agency (ESA) and European GNSS Agency (GSA), Sixth Galileo satellite in corrected orbit. Galileo GNSS online. http://galileognss.eu/tag/galileo-foc-fm1/. Accessed 23 Sep 2015

Guo J, Xu X, Zhao Q, Liu J (2016) Precise orbit determination for quad-constellation satellites at Wuhan University: strategy, result validation, and comparison. J Geod 90:143–159. doi:10.1007/s00190-015-0862-9

IGS-MGEX. Online. http://igs.org/mgex/. Accessed 01 Sep 2016

Ikari S, Ebinuma T, Funase R, Nakasuka S (2013) An evaluation of solar radiation pressure models for QZS-1 precise orbit determination. In: Proceedings of ION GNSS. ION, Nashville, pp 1234–1241

ILRS, Current Missions. Online. http://ilrs.gsfc.nasa.gov/missions/satellite_missions/current_missions/. Accessed 23 Sep 2015

Ishijima Y, Inaba N, Matsumoto A, Terada K, Yonechi H, Ebisutani H, Ukawa S, Okamoto T (2009) Design and development of the first quasizenith satellite attitude and orbit control system. In: Proceedings of the IEEE AerospaceConference, IEEE, pp 1–8. doi:10.1109/AERO.2009.4839537

Konrad A, Fischer HD, Müller C, Oesterlin W (2007) Attitude & orbit control system for Galileo IOV. In: 17th IFAC Symposium on Automatic Control in. Aerospace 2007. doi:10.3182/20070625-5-FR-2916.00006

Kouba J (2009) A simplified yaw-attitude model for eclipsing GPS satellites. GPS Solut 13(1):1–12. doi:10.1007/s10291-008-0092-1

Langley R (2014) ESA discusses galileo satellite power loss. GPS World online. http://gpsworld.com/esa-discusses-galileo-satellite-power-loss-upcoming-launch/. Accessed 23 Sep 2015

Langley R (2016) Navstar GPS Constellation Status. http://www2.unb.ca/gge/Resources/GPSConstellationStatus.txt. Accessed 01 Sept 2016

Lutz S, Arnold D, Schaer S, Dach R, Jäggi A (2013) New RINEX file monitoring at CODE. Poster, EUREF Symposium 2013, Budapest, Hungary, May 29–31 2013

Lutz S, Meindl M, Steigenberger P, Beutler G, Sośnica K, Schaer S, Dach R, Arnold D, Thaller D, Jäggi A (2016) Impact of the arc length on GNSS analysis results. J Geod 90(4):365–378. doi:10.1007/s00190-015-0878-1

MacLeod K, Agrotis L (2013) IGS RINEX Working Group Report 2011. International GNSS Service: Technical Report 2012, edited by Dach R, Jean Y (AIUB), IGS Central Bureau, pp 191–194. doi:10.7892/boris.80303

Montenbruck O, Steigenberger P, Schönemann E, Hauschild A, Hugentobler U, Dach R, Becker M (2012) Flight Characterization of New Generation GNSS Satellite Clocks. Navig J Inst Navig 59(4):291–302

Montenbruck O, Rizos C, Weber R, Weber G, Neilan RE, Hugentobler U (2013) Getting a Grip on Multi-GNSS: The International GNSS Service MGEX Campaign. GPS World 24(7):44–49

Montenbruck O, Steigenberger P, Hugentobler U (2015) Enhanced solar radiation pressure modeling for Galileo satellites. J Geod 89:283–297. doi:10.1007/s00190-014-0774-0

Montenbruck O, Schmid R, Mercier F, Steigenberger P, Noll C, Fatkulin R, Kogure S, Ganeshan AS (2015) GNSS Satellite Geometry and Attitude Models. Adv Space Res 56(6):1015–1029. doi:10.1016/j.asr.2015.06.019

Pearlman MR, Degnan JJ, Bosworth JM (2002) The International Laser Ranging Service. Adv Space Res 30(2):135–143. doi:10.1016/S0273-1177(02)00277-6

Prange L, Dach R, Lutz S, Schaer S, Jäggi A (2016) The CODE MGEX Orbit and Clock Solution. In: Rizos C, Willis P (eds) IAG 150 years, International Association of Geodesy Symposia. Springer, New York, pp 767–773. doi:10.1007/1345_2015_161

Qiao J, Chen W (2015) BeiDou Satellites maneuvers detection for precise Orbit determination. Presentation, 26th IUGG General Assembly, Prague, Czech Republic, 22 June–02 July 2015

Rodriguez-Solano CJ, Hugentobler U, Steigenberger P, Lutz S (2012) Impact of Earth radiation pressure on GPS position estimates. J Geod 86(5):309–317. doi:10.1007/s00190-011-0517-4

Rodriguez-Solano CJ, Hugentobler U, Steigenberger P, Blösfeld M, Fritsche M (2014) Reducing the draconitic errors in GNSS geodetic products. J Geod 88(6):559–574. doi:10.1007/s00190-014-0704-1

Schaer S (2012) Bias and Calibration Working Group: IGS Technical Report 2011. International GNSS Service: Technical Report 2011, edited by Meindl M, Dach R, Jean Y (AIUB), IGS Central Bureau, pp 139–154. doi:10.7892/boris.80302

Sośnica K, Thaller D, Dach R, Steigenberger P, Beutler G, Arnold D, Jäggi A (2015) Satellite laser ranging to GPS and GLONASS. J Geod 89(7):725–743. doi:10.1007/s00190-015-0810-8

Springer TA, Beutler G, Rothacher M (1999) A new solar radiation pressure model for GPS satellites. GPS Solut 3(2):50–62

Springer TA, Flohrer C, Otten M, Enderle W (2014) ESA Reprocessing: Advances in GNSS analysis. Presentation, IGS Workshop 2014, Pasadena, USA, 23–27 June 2014

Steigenberger P, Hugentobler U, Hauschild A, Montenbruck O (2013) Orbit and clock analysis of Compass GEO and IGSO satellites. J Geod 87(6):515–525. doi:10.1007/s00190-013-0625-4

Steigenberger P, Kogure S (2014) IGS-MGEX: QZSS Orbit and Clock Determination. presentation, IGS workshop 2014, Pasadena, USA, 23–27 June 2014

Steigenberger P, Hugentobler U, Loyer S, Perosanz F, Prange L, Dach R, Uhlemann M, Gendt G, Montenbruck O (2015) Galileo orbit and clock quality of the IGS Multi-GNSS Experiment. Adv Space Res 55(1):269–281. doi:10.1016/j.asr.2014.06.030

Steigenberger P, Montenbruck O, Hugentobler U (2015) GIOVE-B solar radiation pressure modeling for precise orbit determination. Adv Space Res 55(5):1422–1431. doi:10.1016/j.asr.2014.12.009

Steigenberger P, Fritsche M, Dach R, Schmid R, Montenbruck O, Uhlemann M, Prange L (2016) Estimation of satellite antenna phase center offsets for Galileo. J Geod 90(8):773–785. doi:10.1007/s00190-016-0909-6

Uhlemann M, Gendt G, Ramatschi M, Deng Z (2016) GFZ Global Multi-GNSS Network and Data Processing Results. In: Rizos C, Willis P (eds) IAG 150 years, International Association of Geodesy Symposia. Springer, New York, pp 673–679. doi:10.1007/1345_2015_120

Ziebart M (2004) Generalized Analytical Solar Radiation Pressure Modeling Algorithm for Spacecraft of Complex Shape. J Spacecr Rocket 41(5):840–848. doi:10.2514/1.13097